MOLECULAR AND CELLULAR BIOLOGY, Apr. 2007, p. 3109–3122 Vol. 27, No. 8
0270-7306/07/$08.00+0 doi:10.1128/MCB.01014-06

The 3BP2 Adapter Protein Is Required for Optimal B-Cell Activation and Thymus-Independent Type 2 Humoral Response▽

Grace Chen,[1,2] Ioannis D. Dimitriou,[2] Jose La Rose,[2] Subburaj Ilangumaran,[3] Wen-Chen Yeh,[4,5]† Gina Doody,[6] Martin Turner,[6] Jennifer Gommerman,[1] and Robert Rottapel[1,2,5,7,8]*

Department of Immunology, University of Toronto, Toronto, Canada[1]; Ontario Cancer Institute, Toronto, Canada M5G 2M9[2]; University of Sherbrooke, North Sherbrooke, Quebec, Canada J1H 5N4[3]; Advanced Medical Discovery Institute, Toronto, Canada M5G 2C1[4]; Department of Medical Biophysics, University of Toronto, Toronto, Canada[5]; Lymphocyte Signaling and Development Laboratory, Molecular Immunology Programme, The Babraham Institute, Babraham, Cambridge CB2 4AT, United Kingdom[6]; Department of Medicine, University of Toronto, Toronto, Canada[7]; and St. Michael's Hospital, 30 Bond St., Toronto, Canada M5B 1W8[8]

Received 6 June 2006/Returned for modification 6 July 2006/Accepted 25 January 2007

3BP2 is a pleckstrin homology domain- and Src homology 2 (SH2) domain-containing adapter protein that is mutated in the rare human bone disorder cherubism and which has also been implicated in immunoreceptor signaling. However, a function for this protein has yet to be established. Here we show that mice lacking 3BP2 exhibited a perturbation in the peritoneal B1 and splenic marginal-zone B-cell compartments and diminished thymus-independent type 2 antigen response. 3BP2$^{-/-}$ B cells demonstrated a proliferation defect in response to antigen receptor cross-linking and a heightened sensitivity to B-cell receptor-induced death via a caspase-3-dependent apoptotic pathway. We show that 3BP2 binds via its SH2 domain to the CD19 signaling complex and is required for optimum Syk phosphorylation and calcium flux.

3BP2 is a pleckstrin homology (PH) domain- and Src homology 2 (SH2) domain-containing adapter protein of unknown function that was originally cloned in a screen to identify c-Abl SH3 binding proteins (4, 33). 3BP2 has been implicated as a positive regulatory adapter molecule coupled to immunoreceptors on T cells (6), B cells (12), NK cells (17), and basophils (35) in overexpression studies. 3BP2 forms complexes with a number of signaling proteins, such as Zap-70, LAT, phospholipase C γ1 (PLC-γ1), Grb2, Cbl, and Fyn in Jurkat cells (6) and Vav1, Vav2, PLC-γ, and Syk in Daudi B cells (12).

Genetic evidence has linked 3BP2 to a rare human disease called cherubism (45). Cherubism is an autosomal dominant disorder characterized by erosion of maxillar and mandibular bone, with resultant dental and facial deformity due to excessive osteoclast activity and giant cell granuloma formation (41). Mutations leading to single amino acid substitutions in 3BP2 have been identified in cherubism patients and map to a six-amino-acid stretch lying between the PH and SH2 domains (45).

Despite the growing body of biochemical data to support the importance of 3BP2 in cells of the hematopoietic lineage, a clear picture of the biological function of 3BP2 has yet to emerge. Here we show that 3BP2$^{-/-}$ mice accumulate splenic marginal-zone (MZ) B cells, possess a reduced frequency of peritoneal B1 B cells, and have a diminished thymus-independent type 2 (TI-2) antigen response. 3BP2$^{-/-}$ B cells demonstrate diminished proliferation and cell survival following cross-linking of the B-cell receptor (BCR). We demonstrate that the endogenous 3BP2 protein binds to the cytoplasmic tail of the B-cell costimulatory molecule CD19 and that 3BP2 deficiency leads to defects in Syk phosphorylation and calcium flux.

MATERIALS AND METHODS

3BP2 gene-targeted mice. The wild-type *3BP2* gene is composed of 13 exons. Exon 2 contains the start codon, exons 2 to 5 encode the PH domain, and exons 10 to 13 encode the SH2 domain of 3BP2. Part of exons 4 and 5 and the intervening intron were deleted. The *3BP2*-targeting vector (Fig. 1A) consisted of a 4-kb homology arm, a 0.9-kb short arm, and a PGK-neomycin cassette (Neo^r). The targeting vector was linearized with SalI and electroporated in the 129/Sv embryonic stem cell line E14. Embryonic stem cells were cultured in selection medium containing G418. The targeted clones were selected and injected into blastocytes from C57BL/6 mice. The chimeric animals were mated with C57BL/6 mice to yield mice that are in the seven-backcross generation (F_7). Mice used in all experiments were in the F_7 backcross generation and were maintained at the animal facilities of the Ontario Cancer Institute under specific-pathogen-free conditions according to University Health Network animal care committee guidelines.

Plasmids. The expression vector of full-length murine 3BP2 was constructed by first amplifying full-length murine 3BP2 by PCR and TA cloning the purified amplified product into PCR2.1 vector (Invitrogen). The 3BP2ΔSH2 construct encoded amino acids (aa) 1 to 461 and lacked sequence encoding the final 98 aa, which includes the SH2 domain. The 3BP2ΔPR plasmid was constructed by cutting pcDNA3.1–full-length 3BP2 with SmaI and BspEI and religating the vector to delete aa 189 to 290. The 3BP2 SH2 R486K construct was generated by overlapping PCR using full-length 3BP2 vector as a template.

Cell culture and transfection. Daudi cells expressing the ΔEC, Y9F, and Y403/443F CD4:CD19 chimeras were gifts from R. Carter (University of Alabama). A20 murine B lymphoma cells were purchased from the American Type Culture Collection (ATCC) and maintained in RPMI medium containing 10% fetal bovine serum, 50 μM β-mercaptoethanol, and 10 mM HEPES. 293T cells (ATCC) were transfected with 4 μg of the indicated plasmids by using Polyfect transfection reagent (QIAGEN) according to manufacturer's recommendations

* Corresponding author. Mailing address: Princess Margaret Hospital/Ontario Cancer Institute, Room 10-105, University Ave., Toronto, ON, Canada M5G 2M9. Phone: (416) 946-4501, ext. 2233. Fax: (416) 946-2984. E-mail: rottapel@oci.utoronto.ca.

† Present address: Amgen San Francisco, 1120 Veterans Boulevard, South San Francisco, CA 94080.

▽ Published ahead of print on 5 February 2007.

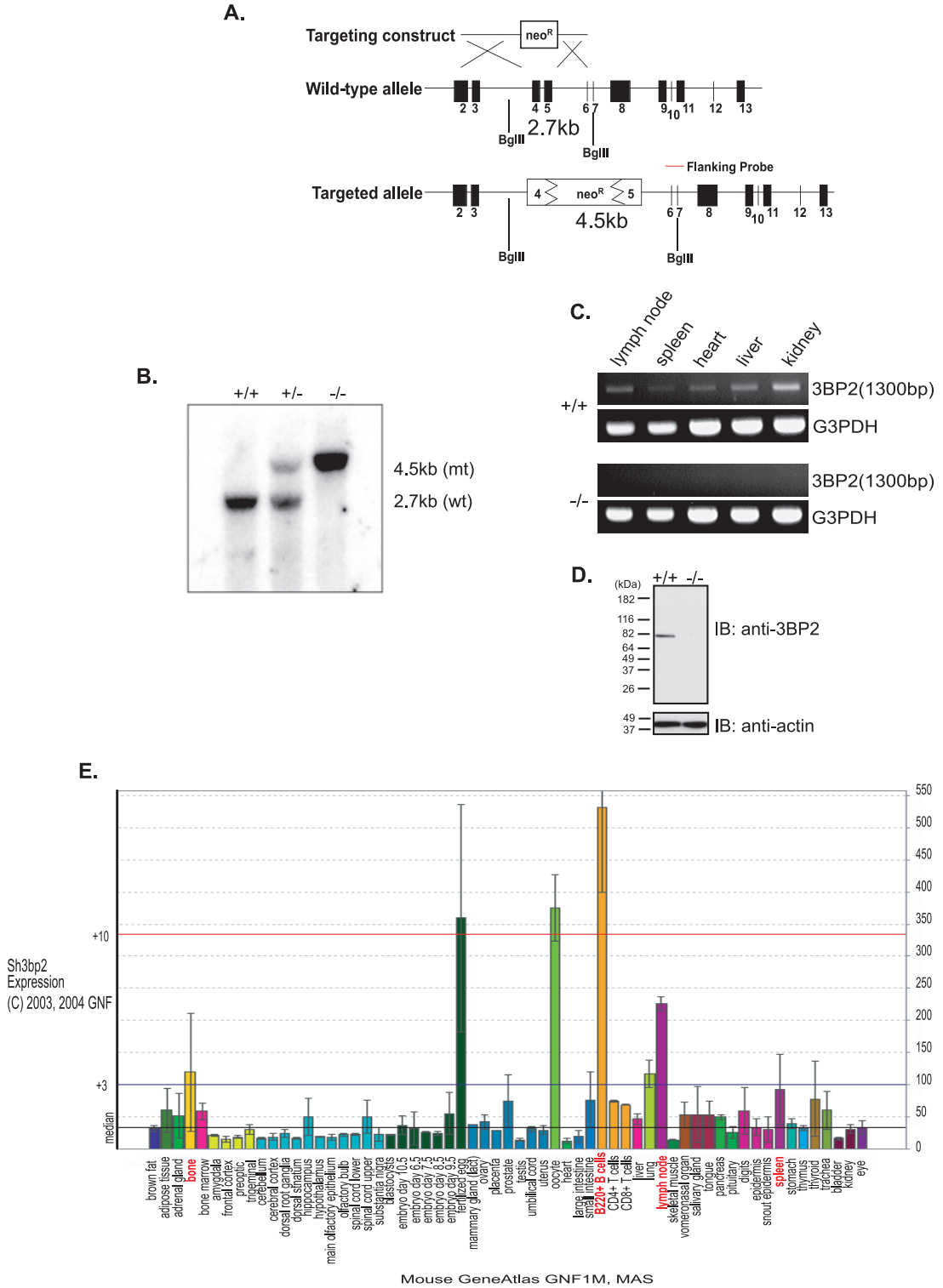

FIG. 1. Generation of 3BP2$^{-/-}$ mice. (A) Schematic diagram of the wild-type *3BP2* gene locus, the targeting vector, and the integrated *3BP2* locus. The wild-type *3BP2* gene is composed of 13 exons. Exon 2 contains the start codon, exons 2 to 5 encode the PH domain, and exons 10 to 13 encode the SH2 domain of 3BP2. Part of exon 4 and 5 and the intervening intron were deleted. The disrupted region lies within the PH domain-coding region. The locations of the flanking probe used for genomic Southern analysis and of the BglII restriction digest sites in the wild-type and mutant alleles are shown. (B) Southern analysis of genomic DNA from 3BP2 wild-type (+/+), heterozygous (+/−), and mutant (−/−) mice. The expected BglII restriction fragment size is shown on the right (mt, mutant; wt, wild-type). (C) Reverse transcription-PCR was performed on mRNAs extracted from different organs of wild-type (+/+) and mutant (−/−) mice. PCR was performed using a primer set flanking exon 5. G3PDH, glyceraldehyde-3-phosphate dehydrogenase. (D) Western analysis of 3BP2 protein expression in purified 3BP2$^{+/+}$ and 3BP2$^{-/-}$ splenic B cells. 3BP2 protein was detected by an antibody directed against the SH2 domain of 3BP2. IB, immunoblotting. (E) Expression of *3BP2* mRNA from different tissues (source, Genomics Institute of Novartis Research Foundation) (42).

and were maintained in medium containing 10% cosmic calf serum, 50 μM β-mercaptoethanol, and 10 mM HEPES. Cells were cultured at 37°C in an incubator with a humidified atmosphere containing 5% CO_2.

Reagents and antibodies. For CD19 and 3BP2 coimmunoprecipitation, the polyclonal antibodies against 3BP2 were prepared following sheep immunization with purified glutathione *S*-transferase (GST)-3BP2 SH2 protein. To verify the absence of protein in 3BP2$^{-/-}$ splenic B cells, we used affinity-purified rabbit polyclonal anti-3BP2 antibody, which was prepared by immunizing rabbits with purified GST-3BP2 SH2 protein (a gift from M. Deckert, Hôpital de l'Archet, Nice, France). The antibodies used in GST pull-down immunoprecipitation and immunoblotting assays were anti-GST (B14 monoclonal antibody [MAb]; Santa Cruz Biotechnology), anti-Flag MAb (M2; Sigma), anti-human CD4 (Caltag), and anti-mouse CD19 (MB19-1; eBioscience). The antibody used in Syk immunoprecipitation was a gift from A. Veillette (McGill University, Montreal, Canada). Anti-PLC-γ2 (Q-20) was purchased from Santa Cruz Biotechnology. 4G10 antibodies were purified from hybridoma supernatant and were used to detect phosphotyrosine residues. Antibodies against phospho-extracellular signal-regulated kinase 1 (Erk1)/Erk2, Erk1/Erk2, phospho-Akt (Ser473), Akt, phospho-Jun N-terminal protein kinase/stress-activated protein kinase (JNK/SAPK), and JNK/SAPK were purchased from Cell Signaling Technology. The biotin-, fluorescein isothiocyanate (FITC)-, phycoerythrin (PE)-, and allophycocyanin (APC)-labeled antibodies used for flow cytometry (all antibodies were from Pharmingen unless otherwise indicated) were anti-B220 (RA3-6B2), anti-CD43 (S7), anti-BP.1 (6C3), anti-HAS (M1/69), anti-CD4 (GK1.5), anti-CD8 (53-6.72), anti-CD25 (7D4), anti-CD44 (1M7), anti-CD3ε (145-2C11), anti-immunoglobulin D (anti-IgD) (SBA.1), anti-μHC (33.60), anti-CD21 (7G6), anti-CD23 (B3B4), and anti-CD5 (53-7.3). Recombinant BAFF used for BAFF-mediated survival assay was purchased from Apotech Corporation (Switzerland).

Isolation of primary lymphocytes. Single-cell suspensions were prepared from spleen. Erythrocytes were lysed in ACK solution (155 mM NH_4Cl, 10 mM $KHCO_3$, 0.1 mM EDTA, 1 N HCl). B lymphocytes were enriched by magnetic cell sorting with anti-CD43 and anti-CD11b MACS microbeads (Miltenyi Biotec), which yielded ~98% B220$^+$ cells. Purified cells were cultured in RPMI medium containing 10% fetal bovine serum, 50 μM β-mercaptoethanol, and 10 mM HEPES.

Flow cytometry analysis and sorting. Single-cell suspension of thymi, lymph nodes, bone marrow, and spleens from 3BP2$^{+/+}$ and 3BP2$^{-/-}$ mice were incubated with Fc block antibodies (2.4G2) at 4°C to minimize nonspecific binding and then stained with a combination of biotin-, FITC-, PE-, APC-labeled antibodies on ice. Biotinylated antibodies were visualized using streptavidin-PE-Cy5. For detection of apoptosis, cultured cells were stained with annexin V and propidium iodide (PI) using an apoptosis detection kit (Pharmingen) according to manufacturer's recommendations. All samples were analyzed by a FACScan or a FACScalibur flow cytometer and analyzed using CellQuest (Becton Dickinson) and Flowjo software.

Splenic B cells were stained with anti-B220–APC (RA3-6B2), anti-CD21–FITC (7G6), and anti-CD23–PE (B3B4) antibodies and then sorted for MZ B cells and follicular (FO) B cells using a MoFlo high-speed cell sorter (Cytomation, Inc.), which yielded ~98 to 99% of MZ B cells and ~94 to 97% of FO B cells.

Immunohistochemistry. Spleens were removed and snap frozen in OCT compound (Thermo Shandon, Pittsburgh, PA). Five-micrometer frozen spleen sections were then generated using a Leica 3050S cryostat, and frozen sections were fixed in ice-cold acetone for 10 min. Spleen sections were first incubated with blocking solution (10% rabbit serum, 10% mouse serum, Fc block antibodies in Tris-buffered saline–0.05% Tween 20) and then stained with biotinylated anti-MAdCAM-1 clone MECA-367 (eBioscience, San Diego, CA) and counterstained with FITC–anti-B220. Sections were then stained with the secondary antibodies streptavidin-conjugated horseradish peroxidase (HRP) (Prozyme, San Leandro, CA) and anti-FITC-conjugated alkaline phosphatase (Roche Diagnostics Canada, Laval, Quebec, Canada). Sections were then developed with a Vector HRP development kit according to the manufacturer's instructions, followed by use of a Vector alkaline phosphatase substrate kit III according to manufacturer's instructions (Vector Laboratories Inc.). Sections were mounted with Crystal/Mount (Biomeda Corp., Foster City, CA) and visualized on a Leica upright DMRA2 microscope.

Immunization. 3BP2$^{+/+}$ and 3BP2$^{-/-}$ mice of 9 weeks of age were immunized intraperitoneally with 25 μg of trinitrophenol conjugated to Ficoll (TNP-Ficoll) or 50 μg TNP-lipopolysaccharide (TNP-LPS) (both from Biosearch Technologies) in sterile phosphate-buffered saline (PBS), and blood was collected at 0, 7, and 14 days postimmunization.

3BP2$^{+/+}$ and 3BP2$^{-/-}$ mice of 8 weeks of age were immunized intraperitoneally with 100 μg TNP-OVA (Biosearch Technologies) in sterile PBS, which was preincubated in Alu-Gel-S (Serva). Blood samples were collected at 0, 7, 14, and 21 days postimmunization.

Enzyme-linked immunosorbent assay (ELISA). For measurement of the concentrations of isotype-specific Igs, each well of 96-well plates was coated with goat anti-mouse Ig as a capture reagent and developed with isotype-specific goat sera directly conjugated with HRP (Southern Biotech).

For anti-TNP and anti-NP ELISAs, each well of 96-well plates was coated with 100 μl of 5-μg/ml bovine serum albumin (BSA)-TNP in PBS for 1 h at 37°C, followed by incubation at 4°C overnight. Plates were blocked with 5% BSA in PBS–0.05% Tween 20 for 2 h at 37°C. The relative quantity of TNP- or NP-specific antibodies in each blood-derived serum sample was determined by isotype-specific ELISA with HRP-conjugated anti-isotype antibodies (Southern Biotech).

Cell proliferation assay. Splenocytes and purified B cells from 8- to 12-week-old mice were stimulated for 48 h with 10 μg/ml F(ab′)$_2$ fragments of anti-mouse IgM (Jackson Immunoresearch) with or without 10 μg/ml anti-CD40 clone 1C10 (Southern Biotech) or 10 μg/ml LPS (*Escherichia coli* 055:B5; Sigma). The cells were harvested onto glass fiber filter mats, and the incorporated radioactivity was measured in a TopCount liquid scintillation counter (Canberra/Packard, Mississauga, Ontario, Canada).

5-Chloromethylfluorescein diacetate labeling of B cells. Purified B cells were loaded with CellTracker Green 5-chloromethylfluorescein diacetate (Molecular Probes) according to the manufacturer's recommendations.

Detection of caspase-3 activity. Immediately after splenocytes were isolated from 3BP2$^{+/+}$ and 3BP2$^{-/-}$ mice, a portion of total splenocytes was incubated with FITC-DEVD-FMK (a caspase-3 inhibitor) according to the manufacturer's recommendations and then stained with antibodies against surface markers B220, CD21, and CD23. B cells were purified from the rest of the splenocytes as described above. Purified B cells were stimulated for 12 and 24 h with 10 μg/ml F(ab′)$_2$ fragments of anti-mouse IgM (Jackson Immunoresearch). At each time point, cells were harvested, incubated with FITC-DEVD-FMK (a caspase-3 inhibitor), and stained for B220, CD21, and CD23.

Intracellular staining of Bcl-x_L, Bcl-2, and Mcl-1. Splenocytes were first stained with antibodies against surface markers B220, CD21, and CD23 and then were permeabilized with permeabilization buffer (Pharmingen) and stained with FITC–anti-Bcl-x_L antibody, PE–anti-Bcl-2 antibody (Pharmingen), or anti-Mcl-1 antibody (rabbit polyclonal; Santa Cruz). PE–anti-rabbit IgG (Jackson Immunoresearch) was used as the secondary antibody to detect Mcl-1. After the unbound antibodies were washed off, cells were fixed with 1% paraformaldehyde (in PBS). B cells were purified from the rest of the unstained splenocytes as described above. Purified B cells were stimulated for 12 and 24 h with 10 μg/ml F(ab′)$_2$ fragments of anti-mouse IgM (Jackson Immunoresearch). At each time point, cells were harvested and stained for B220, CD21, CD23, and intracellular Bcl-x_L, Bcl-2, or Mcl-1.

GST precipitation, immunoprecipitation, and immunoblotting. Cells were lysed in ice-cold 1% NP-40 buffer (1% NP-40, 150 mM NaCl, 50 mM Tris-HCl [pH 8.0], 1 mM sodium orthovanadate, 2 mM EDTA, 50 mM NaF, and protease inhibitors) (13) for 20 min on ice. Nuclei were pelleted by centrifugation for 10 min at 16,000 × *g* and 4°C. For GST precipitations, 10 μg of GST-3BP2 SH2 fusion protein was incubated with glutathione-Sepharose 4B beads (Amersham) for 1 h at 4°C, followed by incubation with lysates for 2 h. Samples were washed four times in lysis buffer. For immunoprecipitation, lysates were incubated for 3 h at 4°C with the indicated antibodies, followed by incubation with either protein A- or protein G-Sepharose beads (Amersham) for 1 h. For CD19-phosphotyrosine peptide precipitation, biotinylated peptides (5 μM) were incubated with 0.2 ml of a 25% slurry of streptavidin-agarose in PBS for 1 h at 4°C, followed by washing. The beads were incubated with NP-40 lysates of 3BP2-transfected 293 cells for 30 min at 20°C. After incubation, pellets were washed three times with ice-cold lysis buffer and resuspended in sodium dodecyl sulfate (SDS) sample buffer (31). For Syk and PLC-γ2 immunoprecipitation, splenic B cells were purified as described above and lysed with cold 1% Triton-X buffer (50 mM HEPES [pH 7], 150 mM NaCl, 10% glycerol, 1% Triton X-100, 1.5 mM $MgCl_2$, 1 mM EGTA, 1 mM Na orthovanadate, 1 mM phenylmethylsulfonyl fluoride, and other protease inhibitors). Antibodies were added to cell lysates, followed by addition of protein A-Sepharose beads (Amersham) beads. Eluted immunoprecipitates or whole-cell lysates were resolved by SDS-polyacrylamide gel electrophoresis (SDS-PAGE), transferred to polyvinylidene difluoride membranes, probed with the indicated primary antibodies and HRP-conjugated secondary antibodies, and developed using an enhanced chemiluminescence kit (Amersham) according to the manufacturer's instructions.

Coimmunoprecipitation. For CD19/3BP2 coimmunoprecipitation from purified splenic B cells, Affigel 10 beads (Bio-Rad) were used and cells were

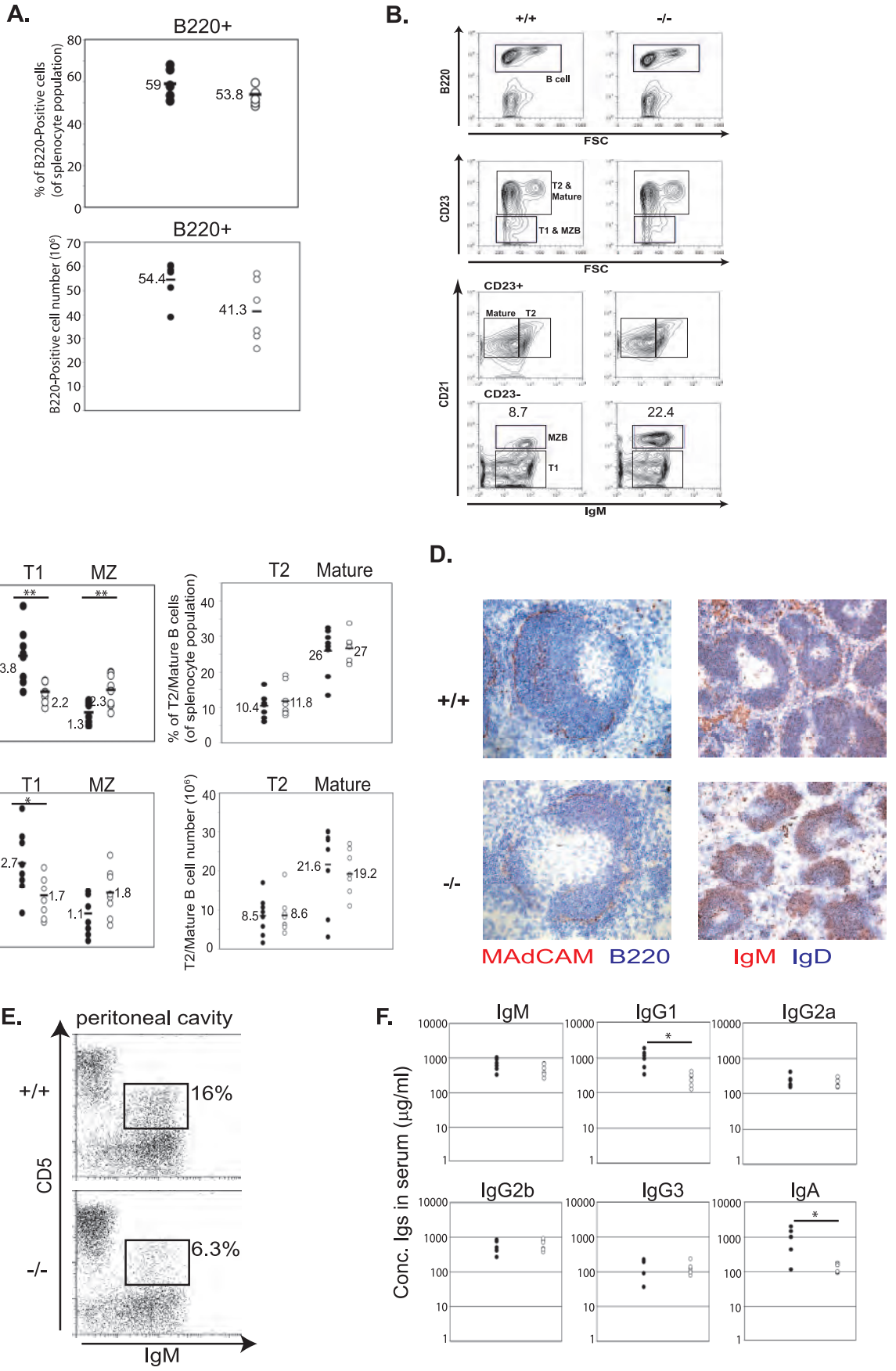
A.
B220+
% of B220-Positive cells (of splenocyte population)
59
53.8
B220+
B220-Positive cell number (10⁶)
54.4
41.3
B.
+/+
-/-
B220
B cell
FSC
CD23
T2 & Mature
T1 & MZB
FSC
CD23+
Mature T2
CD21
CD23-
8.7
22.4
MZB
T1
IgM
C.
T1 MZ
% of T1/MZ B cells (of splenocyte population)
3.8
2.2
1.3
2.3
T2 Mature
% of T2/Mature B cells (of splenocyte population)
10.4
11.8
26
27
T1 MZ
T1/MZ B cell number (10⁵)
2.7
1.7
1.1
1.8
T2 Mature
T2/Mature B cell number (10⁶)
8.5
8.6
21.6
19.2
D.
+/+
-/-
MAdCAM B220
IgM IgD
E.
peritoneal cavity
+/+
16%
CD5
-/-
6.3%
IgM
F.
IgM
IgG1
IgG2a
IgG2b
IgG3
IgA
Conc. Igs in serum (μg/ml)

stimulated with 40 μg/ml of anti-IgM F(ab′)$_2$ in the presence of 10 mM pervanadate.

To determine the domain(s) of 3BP2 required for its binding to CD19, 293T cells transfected with the indicated plasmids were lysed with 1% NP-40 lysis buffer. Lysates were incubated with anti-Flag MAb for 1 h at 4°C, followed by incubation with protein G-Sepharose beads (Amersham) for 2 h. Precipitated products were washed four times with lysis buffer and then added to A20 cell lysates (as a source of endogenous CD19) after A20 cells were stimulated with 20 μg/ml of anti-IgG F(ab′)$_2$. After an 1-h incubation at 4°C, samples were washed and resuspended in SDS sample buffer. Associated proteins were analyzed through immunoblotting as described above.

Calcium flux assay. Resting B cells were purified from 3BP2$^{+/+}$ and 3BP2$^{-/-}$ mice as described above. Purified B cells were washed twice with Hanks balanced salt solution (HBSS). Cells were resuspended at 10×10^6 cells/ml with HBSS (Ca^{2+}, Mg^{2+}, 0.5% BSA). Stock (5 mM in dimethyl sulfoxide) Indo-1AM (Molecular Probes) was diluted to 6 μM and mixed with an equal volume of Pluronic F-120 (20% solution in dimethyl sulfoxide; Molecular Probes). Resuspended cells were mixed with diluted Indo-1AM and Pluronic F-120 at a 1:1 ratio, and the mixture was incubated in a 37°C water bath in the dark for 45 min. After incubation, cells were washed with HBSS twice, and stained for surface markers CD21 and CD23 as described above. Cells were then resuspended at 1×10^6 cells/ml with HEPES-buffered medium (20 mM HEPES [pH 7.4], 140 mM NaCl, 5 mM KCl, 1 mM $MgCl_2$, 1 mM $CaCl_2$, 10 mM glucose) for determination of the concentration of intracellular Ca^{2+} ($[Ca^{2+}]_i$). Measurements were performed using a laser tuned to 338 nm while monitoring emissions at 405 and 450 nm. The $[Ca^{2+}]_i$ was calculated according to the formula (16) $[Ca^{2+}]_i = K_d \times (F_{min}/F_{max}) \times (R - R_{min})/(R_{max} - R)$, where K_d is the dissociation constant for Indo-1 (250 nM at 37°C and pH 7.05), R is the fluorescence intensities measured at 405 and 450 nm during the experiments, and F is the fluorescence intensity measured at 450 nm. R_{min}, R_{max}, F_{min}, and F_{max} were determined from in situ calibration of unlysed cells using 4 μM ionomycin in the absence (R_{min} and F_{min}; 2.5 mM EGTA) and presence (R_{max} and F_{max}) of Ca^{2+}.

Abl kinase assay. Purified 3BP2$^{+/+}$ and 3BP2$^{-/-}$ B cells were stimulated with 10 μg/ml F(ab′)$_2$ fragments of anti-mouse IgM (Jackson Immunoresearch) for the indicated time intervals and were lysed with buffer (25 mM HEPES [pH 7.4], 150 mM NaCl, 3 mM EGTA, 3 mM EDTA, 10% glycerol, 1% Triton X-100, protease inhibitor tablet, 5 mM Na orthovanadate, 10 mM β-glycerophosphate). After 30 min on ice, samples were spun for 10 min at 17,000 × *g* in a microcentrifuge at 4°C. To the supernatants, 2 μg of c-Abl antibody (K12; Santa Cruz Biotechnology) and 20 μl of protein A-Sepharose beads (Amersham) were added and incubated overnight at 4°C. Immune complex were washed three times with ice-cold lysis buffer and twice with ice-cold kinase wash buffer (20 mM HEPES [pH 7.4], 10 mM $MgCl_2$, 1 mM dithiothreitol, 5 mM Na orthovanadate, 10 mM β-glycerophosphate). After the last addition of kinase wash buffer, half of the sample was removed to a fresh tube, which was used for Western blotting to normalize Abl as loading control. To the rest of sample, 20 μl of hot kinase buffer (20 mM HEPES [pH 7.4], 10 mM $MgCl_2$, 1 mM dithiothreitol, 1 mM ATP, 1 μg/ml GST-Crk-mCTD [a gift from the Wang lab, University of California, La Jolla], 20 μl [γ-^{32}P]dATP) was added. The kinase reaction was stopped by addition of 5 μl of 6× sample buffer, and the mixture was boiled for 5 min at 100°C. Samples were resolved on a 12% SDS Tris-glycine gel and then transferred onto polyvinylidene difluoride membranes. The membranes were fixed for 30 min at room temperature in 30% methanol and 10% acetic acid with gentle shaking and dried under vacuum for 2 h at 80°C before being exposed to film to detect radioactivity incorporated into the substrate.

Statistical analysis. Averaged numeric data are represented as means ± standard deviations. Student's *t* test was used to determine the statistical significance of differences between groups.

RESULTS

In order to elucidate the in vivo function of 3BP2, we used homologous recombination to generate 3BP2$^{-/-}$ mice (Fig. 1A) (42). Germ line transmission of the disrupted *3BP2* allele was confirmed by genomic Southern blotting (Fig. 1B) as well as by PCR (data not shown). *3BP2* mRNA was absent in 3BP2$^{-/-}$ tissues (Fig. 1C). The absence of 3BP2 protein in 3BP2$^{-/-}$ mice was verified by Western blotting using an antibody directed against the C terminus of the protein (Fig. 1D). 3BP2$^{-/-}$ mice were born at the expected Mendelian frequency ($n = 292$) and were fertile and viable.

The expression of *3BP2* transcripts in normal mouse tissues as determined by GenAtlas using Affymetrix chip hybridization demonstrated that *3BP2* mRNA expression was restricted to bone, oocytes, lungs, and lymph nodes and that *3BP2* mRNA was most highly expressed in B lymphocytes (Fig. 1E). This pattern of expression was verified by Northern blot analysis (data not shown).

3BP2$^{-/-}$ mice exhibit increased MZ B cells and decreased peritoneal CD5$^+$ B1 B cells. Given the restricted high expression of 3BP2 in B cells, mice lacking 3BP2 were analyzed for possible defects in B-cell development. The frequencies of pre-, immature, and mature recirculating B cells in the bone marrow of 3BP2$^{-/-}$ mice were comparable to those in wild-type controls, whereas we observed a slight decrease of intermediate pro-B cells (B220$^+$ CD43$^+$ BP.1$^-$ HAS$^+$) in mutant mice (~40% versus 34%) (data not shown). Flow cytometric analysis of spleen revealed that the frequency and the absolute number of B220$^+$ splenocytes in the 3BP2$^{-/-}$ mice were comparable to those in wild-type controls (Fig. 2A). We next examined the frequency of splenic B subsets, i.e., transitional-1 (T1) (B220$^+$ CD23$^-$ CD21$^-$ IgM$^+$), transitional-2 (T2) B220$^+$ CD23$^+$ CD21$^+$ IgM$^+$), mature (B220$^+$ CD21$^+$CD23$^+$ IgM$^-$), and MZ (B220$^+$ CD23$^-$ CD21$^+$ IgM$^+$) B cells (Fig. 2B). 3BP2$^{-/-}$ mice had decreased frequency (2.2% ± 0.46% for 3BP2$^{-/-}$ versus 3.8% ± 1.2% for the control) and absolute numbers ($1.7 \times 10^6 \pm 0.67 \times 10^6$ for 3BP2$^{-/-}$ versus $2.7 \times 10^6 \pm 1.1 \times 10^6$ for the control) of T1 cells and a modest increase in frequency (2.3% ± 0.71% for 3BP2$^{-/-}$ versus 1.3% ± 0.5% for the control) and cell numbers ($1.8 \times 10^6 \pm 0.78 \times 10^6$ for

FIG. 2. 3BP2$^{-/-}$ mice have increased MZ B cells, decreased peritoneal B1 B cells, and reduced basal serum IgG1 and IgA levels. (A) The frequency (top panel) and the absolute number (bottom panel) of splenocytes expressing the B220 marker were obtained by fluorescence-activated cell sorter analysis of cells from 3BP2$^{+/+}$ (solid circles) and 3BP2$^{-/-}$ (open circles) mice. Each data point is from an individual mouse, and means are indicated by horizontal lines ($n = 6$). (B) A representative plot of fluorescence-activated cell sorter analysis of subsets of splenic B cells from 3BP2$^{+/+}$ (+/+) and 3BP2$^{-/-}$ (−/−) mice. Antibodies against surface markers B220, IgM, CD23, and CD21 were used to distinguish between different subsets of splenic B cells. 3BP2$^{-/-}$ mice show a 2.5-fold increase in MZ B cells. (C) Frequency (top panels) and absolute numbers (lower panels) of subsets of splenic B cells were obtained based on fluorescence-activated cell sorter analysis of cells from 3BP2$^{+/+}$ (solid circles) and 3BP2$^{-/-}$ (open circles) mice. Each data point is from an individual mouse, and means are indicated by horizontal lines ($n = 8$; *, $P < 0.05$; **, $P < 0.01$). (D) Cryosections of spleens from 3BP2$^{+/+}$ (+/+, top panels) and 3BP2$^{-/-}$ (−/−, bottom panels) were stained with antibodies against MAdCAM-1 (red) plus B220 (blue) and with antibodies against IgM (red) plus IgD (blue). Anti-MAdCAM-1 stains the marginal sinus of spleen (21). The data shown are representative of three independent experiments. (E) Cells recovered from peritoneal washes were stained with antibodies against IgM and CD5 to compare the relative numbers of B1 B cells (IgM$^+$ CD5$^+$) in 3BP2$^{+/+}$ and 3BP2$^{-/-}$ mice. The data shown are representative of three independent experiments. (F) Sera were collected from 9- to 11-week-old 3BP2$^{+/+}$ and 3BP2$^{-/-}$ mice and measured for the concentrations of each Ig isotype by standard ELISA ($n = 6$; *, $P < 0.05$).

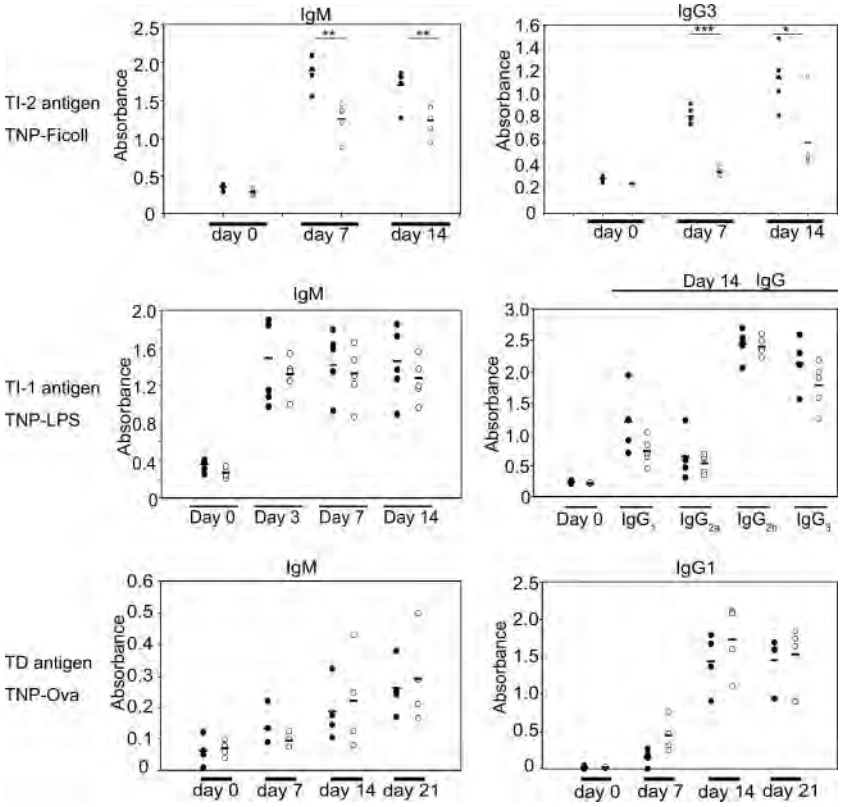

FIG. 3. Humoral response in 3BP2$^{-/-}$ mice. 3BP2$^{+/+}$ and 3BP2$^{-/-}$ mice were immunized with the TI-2 antigen TNP-Ficoll and the TI-1 antigen TNP-LPS. Serum anti-TNP antibodies in 3BP2$^{+/+}$ (solid circles) and 3BP2$^{-/-}$ (open circles) mice were measured by ELISA at 0, 7, and 14 days postimmunization ($n = 5$; *, $P < 0.05$; **, $P < 0.01$; ***, $P < 0.001$). 3BP2$^{+/+}$ and 3BP2$^{-/-}$ mice were also immunized with the T-dependent antigen TNP-OVA. Serum anti-TNP antibodies in 3BP2$^{+/+}$ (solid circles) and 3BP2$^{-/-}$ (open circles) mice were measured by ELISA at 0, 7, 14, and 21 days postimmunization ($n = 4$).

3BP2$^{-/-}$ versus $1.1 \times 10^6 \pm 0.66 \times 10^6$ for the control) of MZ B cells. T2 and mature B cells were not perturbed in 3BP2$^{-/-}$ mice (Fig. 2C).

We performed immunohistochemistry to determine whether splenic architecture was altered in 3BP2$^{-/-}$ mice. Many follicles manifested enlargement of the MZ compartment as delineated by B220$^+$ cells populating the region outside of the marginal sinus (Fig. 2D) (21). Many of the cells within the MZ stained positive for IgM$^+$ IgD$^-$, which is indicative of increased numbers of MZ B cells in this expanded compartment (Fig. 2D). In distinction to MZ B cells, CD5$^+$ IgM$^+$ peritoneal B1 B cells were significantly diminished in the 3BP2$^{-/-}$ mice compared to 3BP2$^{+/+}$ mice (6.3% ± 2% for 3BP2$^{-/-}$ versus 16% ± 0.57% for the control) (Fig. 2E). Serum antibody levels from naïve mice were measured by ELISA, demonstrating significantly reduced levels of IgG1 and IgA but not the other isotypes of Igs in 3BP2$^{-/-}$ mice (Fig. 2F). No T-cell developmental abnormalities were detected within the thymus or lymph node in 3BP2$^{-/-}$ mice (data not shown).

These data suggest that 3BP2 deficiency gave rise to B-cell-specific abnormalities characterized by diminished numbers of immature T1 B cells, an expanded MZ B-cell pool, a contracted CD5$^+$ peritoneal B1 B-cell population, and reduced basal serum IgG1 and IgA levels.

Impaired TI-2 response in immunized 3BP2$^{-/-}$ mice. MZ B cells and B1 B cells have been linked to immune responses to TI-2 multivalent antigens (22, 25). We tested the capacity of the 3BP2$^{-/-}$ mice to elicit a TI-2 humoral response. 3BP2$^{-/-}$ mice were challenged with TNP-Ficoll, a classical T-cell-independent antigen (27). Serum anti-TNP antibodies in 3BP2$^{-/-}$ mice and wild-type controls were measured by ELISA following i.p. injection of TNP-Ficoll at 7 and 14 days postimmunization. Compared to wild-type mice, 3BP2$^{-/-}$ mice produced significantly lower titers of anti-TNP IgM and IgG3 antibodies following immunization (Fig. 3, top panels). In distinction to the TI-2 immune response, 3BP2$^{-/-}$ mice were fully competent to elicit TI-1 and T-dependent immune responses to TNP-LPS or TNP-Ova, respectively (Fig. 3, middle and lower panels). These data show that 3BP2, as an adapter protein, is required for the functional response of B cells to TI-2 antigen challenge.

Impaired proliferation and survival of 3BP2$^{-/-}$ splenic B cells. We next tested the requirement of 3BP2 in sorted resting splenic B cells to mediate proliferation and survival following BCR cross-linking with anti-IgM antibody and LPS exposure. Purified splenic B cells were stimulated with either anti-IgM, anti-IgM plus anti-CD40, or LPS. Forty-eight hours after stimulation, the proliferation index of the B cells was measured by [^{3}H]thymidine incorporation. 3BP2$^{-/-}$ resting B cells showed a lower proliferative response following cross-linking with anti-IgM or anti-IgM plus anti-CD40 antibodies compared to control 3BP2$^{+/+}$ B cells, while the LPS response was normal in

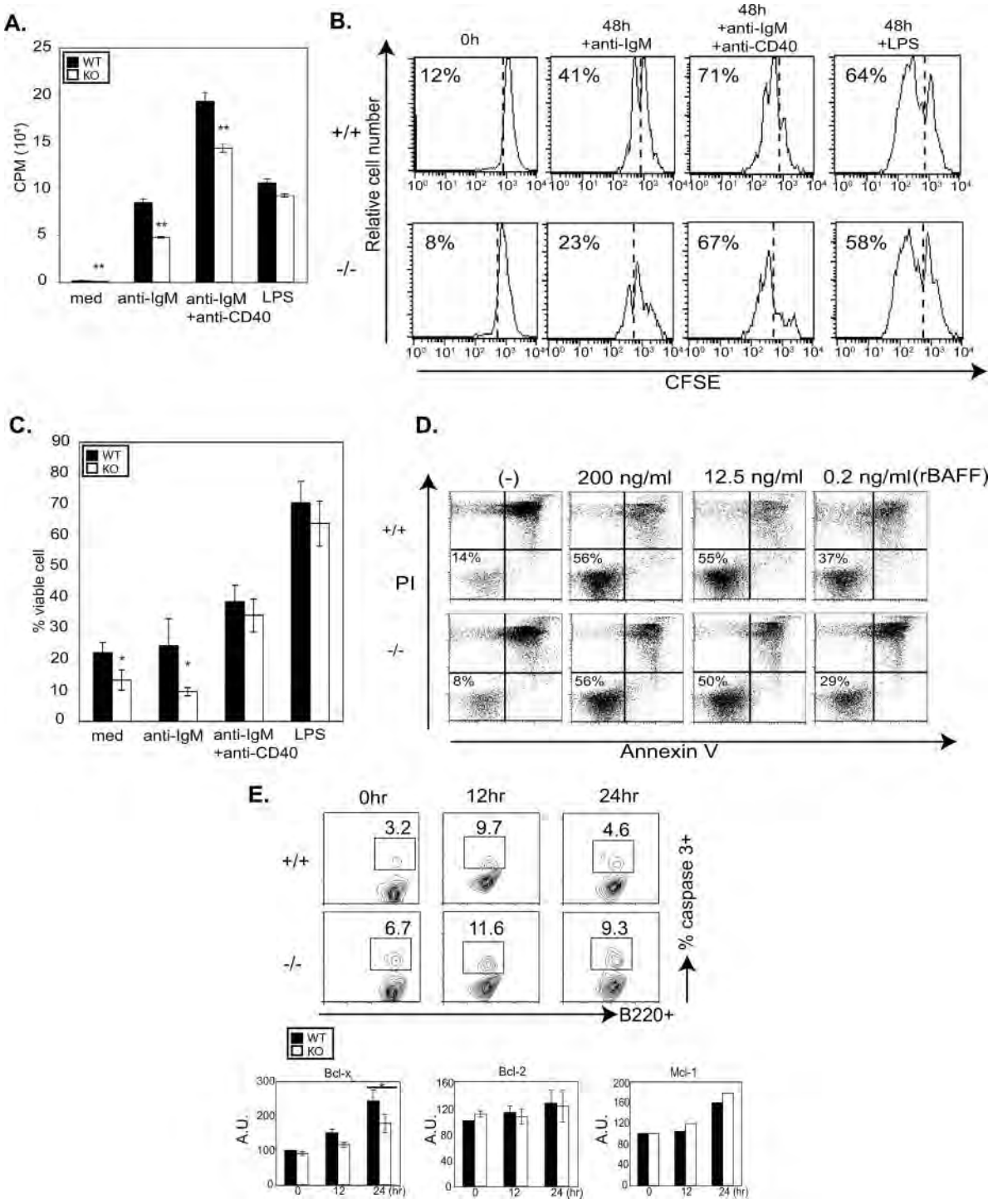

FIG. 4. The BCR-mediated proliferation and cell viability of 3BP2$^{-/-}$ resting B cells are reduced. (A) Purified B cells from 3BP2$^{+/+}$ (WT) and 3BP2$^{-/-}$ (KO) mice were treated as indicated. Wells of a 96-well plate were pulsed with [^{3}H]thymidine (1 μCi/well), and DNA synthesis during the final 12 h of culture was measured by liquid scintillation counting. The data presented are the means and standard deviations from triplicate wells and are representative of three independent experiments (**, $P < 0.01$). med, medium. (B) Purified B cells were labeled with carboxyfluorescein succinimidyl ester (CFSE) and treated as indicated. Cell division was determined for viable cells. The data shown are representative of three independent experiments. (C) Purified 3BP2$^{+/+}$ and 3BP2$^{-/-}$ B cells were treated as indicated, and the percentage of cells negative for both annexin V binding and PI staining was measured after 48 h. The values are averages and standard deviations for four individual animals of each genotype ($n = 4$; *, $P < 0.05$) from four independent experiments. (D) Purified 3BP2$^{+/+}$ and 3BP2$^{-/-}$ B cells were treated with different concentrations of recombinant BAFF (rBAFF) (200, 12, and 0.2 ng/ml) for 72 h. The percentage of the viable cells negative for both annexin V binding and PI staining is shown. The data shown are representative of three separate experiments. (E) Enhanced activation of caspase-3 in 3BP2$^{-/-}$ splenic B cells ex vivo, 12 h and 24 h after BCR cross-linking, compared to that in 3BP2$^{+/+}$ cells. The data shown are representative of five separate experiments. Numbers indicate the percentage of B220$^+$ cells with activated caspase-3. The lower panels show decreased up-regulation of antiapoptotic Bcl-x_L molecules in 3BP2$^{-/-}$ B cells at 24 h after BCR cross-linking compared to 3BP2$^{+/+}$ B cells. In contrast, Mcl-1 and Bcl-2 expression following BCR cross-linking was comparable in control and mutant cells (*, $P < 0.05$). A.U., arbitrary units.

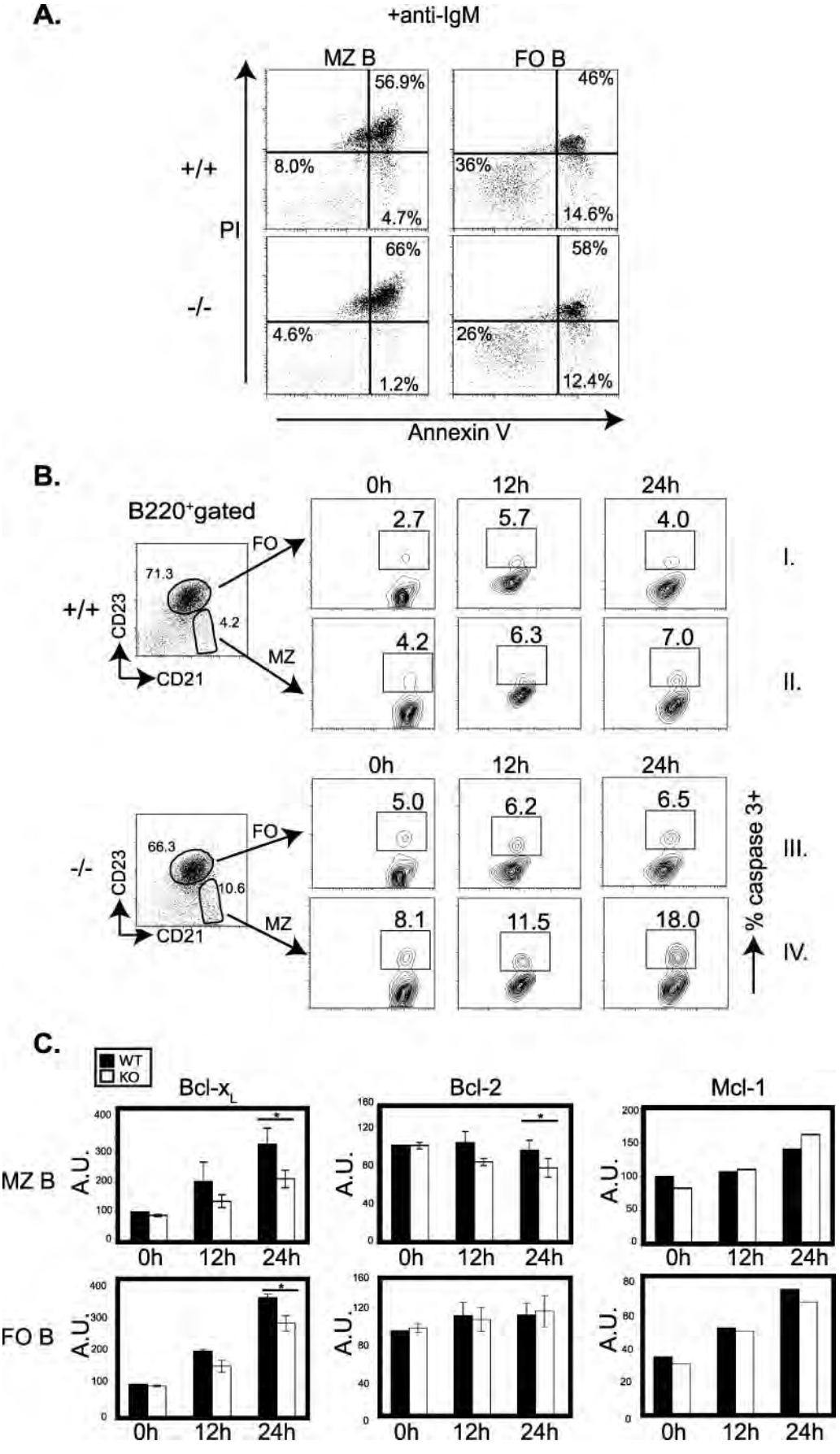
A.
+anti-IgM
MZ B
FO B
56.9%
46%
+/+
8.0%
36%
4.7%
14.6%
PI
66%
58%
-/-
4.6%
26%
1.2%
12.4%
Annexin V
B.
0h
12h
24h
B220+gated
2.7
5.7
4.0
FO
71.3
+/+
CD23
4.2
MZ
CD21
I.
4.2
6.3
7.0
II.
0h
12h
24h
5.0
6.2
6.5
66.3
FO
-/-
CD23
10.6
MZ
CD21
III.
8.1
11.5
18.0
% caspase 3+
IV.
C.
WT
KO
Bcl-xL
Bcl-2
Mcl-1
MZ B
FO B
A.U.
0h
12h
24h

3BP2$^{-/-}$ B lymphocytes (Fig. 4A). To determine if the diminished incorporation rates of [^{3}H]thymidine observed in the 3BP2$^{-/-}$ B cells resulted from their decreased capacity to undergo cell division or an increased tendency to undergo cell death, cells were analyzed by the carboxyfluorescein succinimidyl ester dilution assay or annexin V/PI staining following stimulation with anti-IgM, anti-IgM plus anti-CD40, or LPS. At 48 hours after stimulation a smaller fraction of 3BP2$^{-/-}$ B cells than of 3BP2$^{+/+}$ B cells completed the first cell division in response to BCR cross-linking (23% versus 41%) (Fig. 4B). This delay in cell division was less prominent following CD40 costimulation or treatment with LPS. The viability of 3BP2$^{-/-}$ B cells was also significantly diminished in medium alone and following BCR cross-linking relative to that of 3BP2$^{+/+}$ B cells at 48 h (Fig. 4C). The 3BP2$^{-/-}$ B-cell survival defect was largely corrected by anti-CD40, LPS, or BAFF stimulation (Fig. 4C and D).

To determine whether the defect in cell survival of 3BP2$^{-/-}$ B cells was due to accelerated apoptosis, we examined the activation of caspase-3 following BCR cross-linking. Purified B cells were stimulated with anti-IgM antibodies for 12 and 24 h, and the percentage of cells with active caspase-3 was determined with an FITC-conjugated cell-permeative, nontoxic inhibitor (FITC-DEVD-FMK) that binds irreversibly to activated caspase-3 in apoptotic cells. At 24 h, 3BP2$^{-/-}$ B cells demonstrated a twofold-increased frequency of caspase-3 activation compared to the 3BP2$^{+/+}$ B cells (Fig. 4E).

The regulation of the intrinsic cell death pathway in B cells is controlled by the balanced expression of antiapoptotic proteins Bcl-x$_L$ (10), Bcl-2 (14), Mcl-1 (30), and A1 (15). We examined the capacity of 3BP2$^{+/+}$ and 3BP2$^{-/-}$ B cells to appropriately up-regulate Bcl-x$_L$, Bcl-2, and Mcl-1 in comparison to the 3BP2$^{+/+}$ B cells following BCR cross-linking. Purified resting B cells were stimulated with anti-IgM antibodies for 12 or 24 h, fixed, and stained with anti-Bcl-x$_L$, anti-Bcl-2, or anti-Mcl-1 antibodies. Compared to 3BP2$^{+/+}$ B cells, there was a lag in Bcl-x$_L$ up-regulation in 3BP2$^{-/-}$ B cells 24 h following BCR cross-linking, whereas both 3BP2$^{+/+}$ and 3BP2$^{-/-}$ B cells were equally competent to up-regulate other antiapoptotic molecules such as Bcl-2 and Mcl-1 in response to BCR cross-linking (Fig. 4E). These experiments show that resting B cells derived from 3BP2$^{-/-}$ mice demonstrate both a proliferation defect and a survival defect in response to stimulation through BCR and suggest that 3BP2 is required for optimal BCR signal transduction.

Impaired survival of 3BP2-deficient MZ B cells. FO and MZ B cells respond differently to BCR signals. Cross-linking of the BCR induces proliferation and survival in FO B cells, while MZ B cells undergo programmed cell death induction in in vitro studies (29), suggesting that these related cell types may be wired differently. To test whether 3BP2 plays a selective role in BCR-mediated outcomes in peripheral B-cell subsets, we assessed the susceptibility of FO and MZ B cells from 3BP2$^{+/+}$ and 3BP2$^{-/-}$ mice to undergo antigen receptor-induced death. In concert with previous findings, we observed an increased sensitivity of wild-type MZ B cells to undergo antigen receptor-induced cell death compared to FO B cells (Fig. 5A, top panels) (8% versus 36% viable cells, respectively, at 24 h). However, we observed a differential sensitivity to antigen receptor-induced cell death in the MZ B-cell compartment compared to FO B cells in the absence of 3BP2. Specifically, MZ B cells experienced a 42% decrease in viability compared to FO B cells, whose viability diminished by only 28% in the absence of 3BP2 compared to wild-type controls (Fig. 5A). Moreover, by 24 h nearly all of the nonviable 3BP2$^{-/-}$ MZ B cells had entered the late apoptotic stage (annexin V$^+$ PI$^+$) compared to wild-type MZ B cells, suggesting that in the absence of 3BP2, MZ B cells have an enhanced rate of apoptosis (Fig. 5A, left panels). Addition of anti-CD40 MAbs, LPS, or BAFF to the culture system rescued the death phenotype of wild-type and knockout B cells from both compartments (data not shown).

Given the exquisite sensitivity to antigen receptor-mediated death observed in the 3BP2$^{-/-}$ MZ B cells, we measured caspase-3 activation in MZ B cells (B220$^+$ CD21^{hi} CD23$^-$) compared with FO B cells (B220$^+$ CD21$^+$ CD23$^+$) derived from 3BP2$^{+/+}$ and 3BP2$^{-/-}$ mice. Whereas 3BP2$^{-/-}$ FO B cells showed a moderate increase in the frequency of caspase-3 activation compared to 3BP2$^{+/+}$ FO B cells (Fig. 5B, panel III versus panel I), 3BP2$^{-/-}$ MZ B cells demonstrated a 2.5-fold-increased frequency of caspase-3 activation compared to the normal MZ B cells (Fig. 5B, panel IV versus panel II).

We examined the capacity of 3BP2$^{+/+}$ and 3BP2$^{-/-}$ MZ B cells to up-regulate the antiapoptotic proteins Bcl-x$_L$, Bcl-2, and Mcl-1 following BCR cross-linking by flow cytometry. 3BP2$^{-/-}$ MZ B cells failed to optimally express Bcl-x$_L$ and Bcl-2 at both 12 and 24 h following BCR cross-linking compared to 3BP2$^{+/+}$ controls, whereas Mcl-1 protein induction was not affected by the absence of 3BP2 (Fig. 5C, upper panels). 3BP2$^{-/-}$ FO B cells also demonstrated a defect in Bcl-x$_L$ induction, whereas induction of both Bcl-2 and Mcl-1 was comparable to that of controls following BCR cross-linking (Fig. 5C, lower panels). Therefore, FO and MZ B cells demonstrate a differential requirement for 3BP2 for the proper up-regulation of the Bcl-x$_L$ and Bcl-2 antiapoptotic proteins in response to antigen receptor stimulation.

The 3BP2 signaling complex. 3BP2 interacts with a number of signaling molecules in hematopoietic cells, including Abl (40), Syk (6), and Vav and PLC-γ (12). Moreover, overexpression of 3BP2 stimulates the JNK (19) and Erk mitogen-activated protein kinase pathways (34). In order to determine the biochemical defect underlying the B-cell abnormality observed

FIG. 5. The cell viability of 3BP2$^{-/-}$ MZ B cells is reduced after BCR cross-linking. (A) Purified 3BP2$^{+/+}$ (top panels) and 3BP2$^{-/-}$ (lower panels) MZ B cells (left panels) and FO B cells (right panels) were treated as indicated, and the percentage of cells negative for both annexin V binding and propidium iodide staining was measured after 24 h. The data presented are representative of three separate experiments. (B) Enhanced activation of caspase-3 in 3BP2$^{-/-}$ MZ B cells (panel IV) and FO B cells (panel III) ex vivo, 12 h and 24 h after BCR cross-linking, compared to that in 3BP2$^{+/+}$ cells (panels I and II). Numbers indicate the percentages of MZ B and FO B cells with activated caspase-3. The data shown are representative of five independent experiments. (C) Decreased up-regulation of Bcl-x$_L$ and Bcl-2 in 3BP2$^{-/-}$ MZ B cells (KO) 24 h after BCR cross-linking compared to that in 3BP2$^{+/+}$ MZ B cells (WT) and decreased up-regulation of Bcl-x$_L$ in 3BP2$^{-/-}$ FO B cells 24 h after BCR cross-linking compared to that in 3BP2$^{+/+}$ FO B cells. In contrast, Mcl-1 expression following BCR cross-linking was comparable in control and mutant cells ($*$, $P < 0.05$). A.U., arbitrary units.

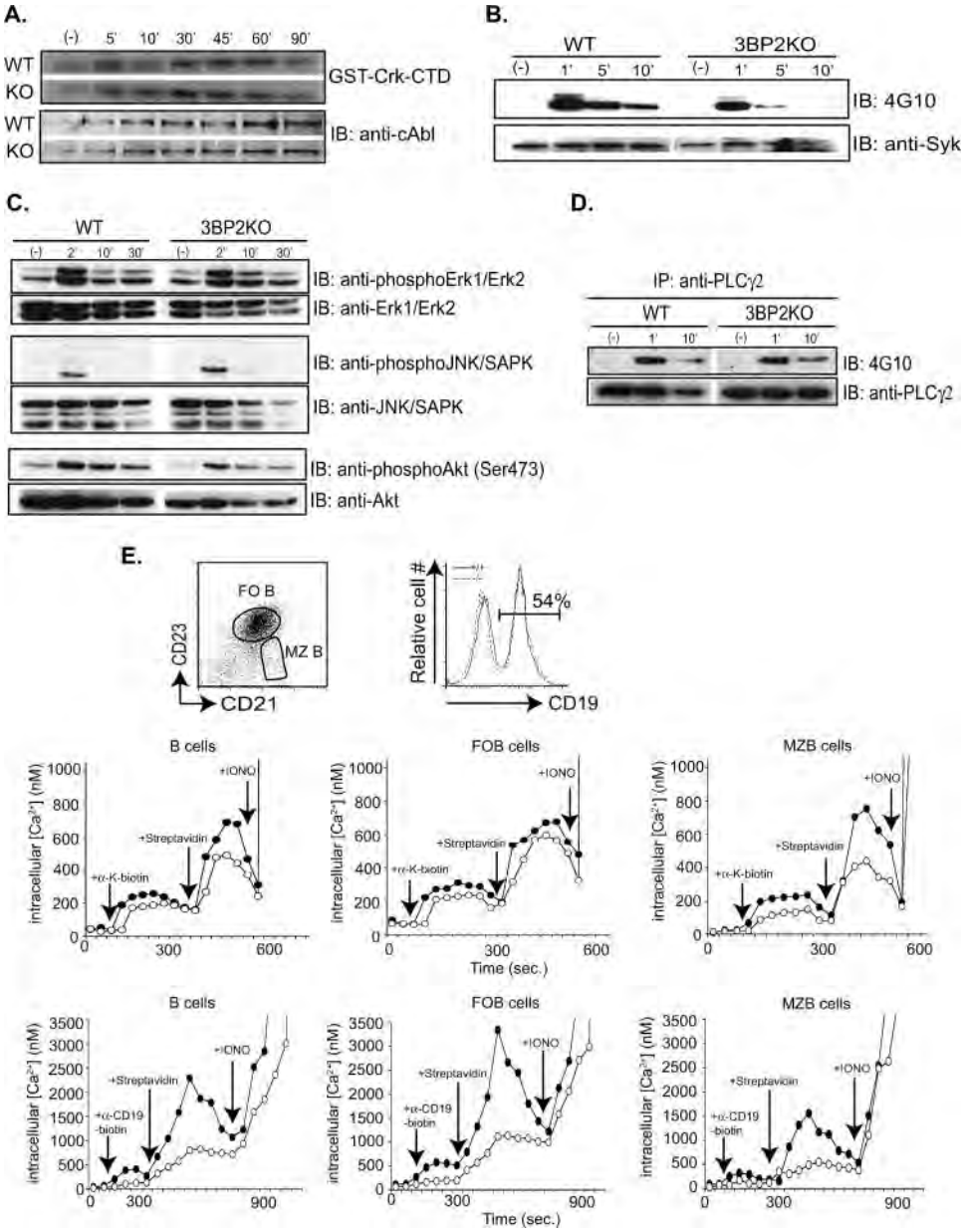

FIG. 6. The 3BP2 signaling complex. (A) The kinase activity of c-Abl was determined for c-Abl immunoprecipitated from either $3BP2^{+/+}$ (WT) or $3BP2^{-/-}$ (KO) splenic B cells using GST-Crk-mCTD as a substrate (top panels). Abl protein was detected with anti-Abl antibody (bottom panels). (B) Kinetics and magnitude of immunoprecipitated Syk tyrosine phosphorylation following BCR cross-linking in $3BP2^{+/+}$ and $3BP2^{-/-}$ splenic B cells. IB, immunoblotting. (C) Cell lysates from $3BP2^{+/+}$ and $3BP2^{-/-}$ splenic B cells unstimulated or stimulated with 10 μg/ml of anti-IgM $F(ab')_2$ were resolved by SDS-PAGE and probed with phosphospecific antibodies against phospho-Erk1/2, -JNK/SAPK, and -Akt. The same membrane was stripped and reprobed with anti-Erk1/2, -JNK/SAPK, and -Akt. (D) Resting splenic $3BP2^{+/+}$ and $3BP2^{-/-}$ B cells were either left unstimulated or stimulated with 10 μg/ml of anti-IgM $F(ab')_2$ for indicated time intervals at 37°C before lysis. PLC-γ2 was immunoprecipitated (IP), resolved by SDS-PAGE, and probed with antiphosphotyrosine antibody 4G10, and the same membrane was stripped and reprobed with anti-PLC-γ2. (E) Indo-1-loaded splenic B cells, with surface staining of CD21 and CD23, were analyzed for ~120 s before stimulation with biotinylated Fab antibody to κ light chain of BCR at 10 μg/ml (upper graphs) or with biotinylated $F(ab')_2$ antibody to CD19 at 10 μg/ml (lower graphs). Cross-linking of BCR or super-cross-linking of CD19 was done with addition of 20 μg/ml of streptavidin. Distinction between total, FO, and MZ B cells was based on CD23 and CD21 surface staining. Calculation of $[Ca^{2+}]_i$ was as described in Materials and Methods. Changes of $[Ca^{2+}]_i$ following BCR cross-linking (upper graphs) and CD19 super-cross-linking (lower graphs) are shown with arrows indicated the addition of each stimulus. $3BP2^{+/+}$ cells are represented by solid circles, and $3BP2^{-/-}$ cells are represented by open circles. The data shown are representative of four independent experiments. Equal levels of CD19 expression on $3BP2^{+/+}$ and $3BP2^{-/-}$ splenocytes were verified using FITC-conjugated anti-CD19 antibody.

in the $3BP2^{-/-}$ mice, we analyzed the phosphorylation status of several of these signaling pathways. The Abl tyrosine kinase is activated following BCR cross-linking (51) and binds to the polyproline region of 3BP2 through its SH3 domain (33). Since Abl is maintained in an autoinhibited state by the intramolecular interaction of the Abl SH3 domain and the linker region (28), binding of 3BP2 to the Abl SH3 might stimulate Abl kinase activity. We performed an Abl in vitro kinase assay with

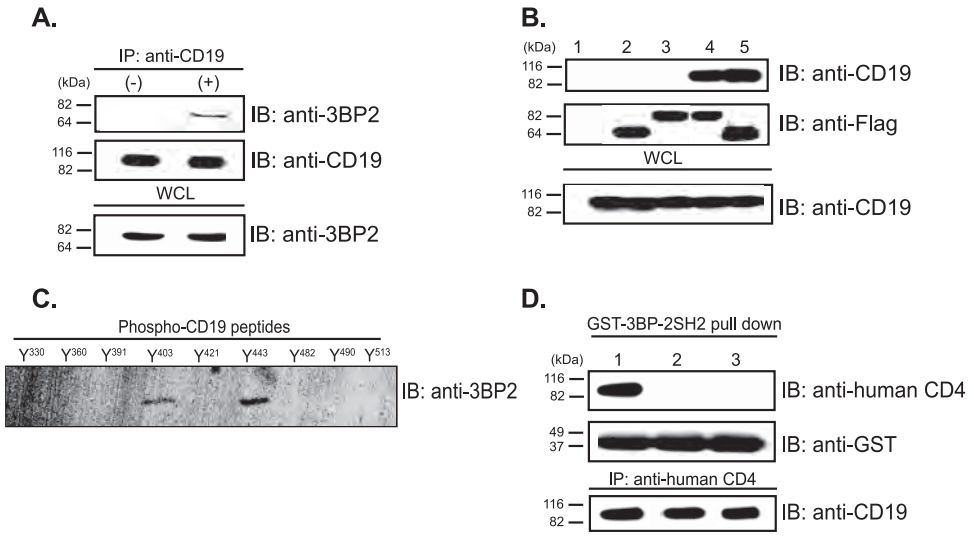

FIG. 7. 3BP2 forms an inducible complex with CD19 via SH2-phosphotyrosine interaction following BCR cross-linking. (A) Inducible binding between CD19 and 3BP2 was demonstrated by coimmunoprecipitation (IP) of endogenous CD19 and 3BP2 from stimulated (with 40 μg/ml of anti-IgM F(ab′)$_2$) 3BP2$^{+/+}$ splenic B cells. IB, immunoblotting; WCL, whole-cell lysate. (B) Untransfected 293T cells (lane 1) and 293T cells transfected with Flag-3BP2 ΔSH2 (lane 2), Flag-3BP2 SH2^{R486K} (lane 3), Flag-3BP2 (lane 4), and Flag-3BP2 ΔPR (lane 5) were used to determine the region(s) of 3BP2 required for its inducible interaction with CD19. A20 cells were used as the source of endogenous CD19. (C) Streptavidin-agarose beads coated with 11-mer biotinylated phosphotyrosyl peptides corresponding to sequences in the cytoplasmic domain of human CD19 [PQNQY*(^{330})GNVLSL, TAPSY*(^{360})GNPSSD, EGEGY*(^{391})EEPDSE, DSEFY*(^{403})ENDSNL, DGSGY*(^{421})ENPEDE, NAESY*(^{443})ENEDEL, GSQSY*(^{482})EDMRGI, RGILY*(^{490})AAPQLR, and DADSY*(^{513})ENMDNP] (43), were incubated with lysates of 3BP2-transfected 293 cells, and adsorbed proteins were eluted, resolved by SDS-PAGE, transferred to an Immobilon membrane, and immunoblotted with antibody to 3BP2, followed by enhanced chemiluminescence. (D) Daudi B lymphoblastoid cells expressing CD4:CD19 chimeric receptors of ΔEC, in which the extracellular domain of CD19 was replaced with that of human CD4 (26) (lane 1); Y9F, in which all nine tyrosines present in the cytoplasmic tail have been replaced with phenylalanine (lane 2); or Y403/443F, in which phenylalanine was substituted for tyrosines 403 and 443 in the cytoplasmic domain (23) (lane 3) were stimulated with F(ab′)$_2$ goat antibody to IgM. The chimeric receptors were precipitated from cell lysates by incubation with GST-3BP2 SH2. The chimeric receptors were detected by antibodies against human CD4. The membrane was stripped and reprobed with anti-GST antibodies. The presence of CD4:CD19 chimeric receptors in each cell lines was confirmed by immunoprecipitation with antibody against human CD4 and immunoblotting with antibody against CD19.

the exogenous Abl substrate GST-Crk-mCTD (50) on purified B cells from 3BP2$^{+/+}$ and 3BP2$^{-/-}$ mice to determine if the induction of Abl kinase activity is defective in cells lacking 3BP2. The induction of Abl kinase activity following BCR cross-linking was similar in amplitude and kinetics in both 3BP2$^{+/+}$ and 3BP2$^{-/-}$ B cells (Fig. 6A).

3BP2 was also identified as a Syk kinase binding protein (6). We examined the induction of Syk tyrosine phosphorylation following BCR cross-linking. Immunoprecipitated Syk was rapidly and maximally tyrosine phosphorylated at 1 minute following BCR cross-linking in 3BP2$^{+/+}$ B cells. However, Syk phosphorylation was significantly reduced in B cells lacking 3BP2, with no detectable signal after 5 min of stimulation (Fig. 6B). These data demonstrate that 3BP2 is required for maximal induction and sustained duration of Syk tyrosine phosphorylation following BCR activation. Importantly, other downstream targets of BCR activation, such as Erk, JNK, Akt, and PLC-γ2, were not affected by 3BP2 deficiency (Fig. 6C and D). Lastly, we measured the absolute concentration of intracellular calcium in B cells lacking 3BP2 by using the cell-permeative fluorescent dye Indo-1 and observed a 30% reduction in calcium levels following BCR cross-linking compared to that in control cells. We observed a differential requirement for 3BP2 between FO and MZ B cells for an optimal induction of calcium influx following BCR cross-linking. Whereas there was only a slight difference in the intracellular calcium concentration between 3BP2$^{-/-}$ and wild-type FO B cells, 3BP2$^{-/-}$ MZ B cells showed a twofold reduction in maximum calcium levels following BCR cross-linking compared to those in wild-type MZ B cells (400 nM versus 800 nM) (Fig. 6E, upper panels). We noted in that response to CD19 super-cross-linking the calcium flux in 3BP2$^{-/-}$ FO and MZ B cells was reduced by more than half of that observed in normal B cells, suggesting that 3BP2 may be important in CD19 signal transduction (Fig. 6E, lower panels). This difference was not attributable to differences in CD19 surface expression, as the wild-type and 3BP2$^{-/-}$ B cells express similar levels of CD19 (Fig. 6E).

The cytoplasmic tail of CD19 contains four possible 3BP2 SH2 domain binding sites (40, 49). We investigated whether 3BP2 could form an inducible and stable complex with CD19 in splenic B cells and found that endogenous 3BP2 binds to CD19 following BCR cross-linking (Fig. 7A). Mutants of 3BP2 either lacking the SH2 domain or harboring a loss-of-function mutation in the SH2 domain did not bind to CD19 (Fig. 7B), which demonstrated that 3BP2 binds to CD19 through its SH2 domain in a tyrosine phosphorylation-dependent manner. We used streptavidin-agarose beads coated with each of nine biotinylated 11-mer peptides containing phosphotyrosine and flanking sequences corresponding to the cytoplasmic domain of human CD19 (43) to map the interaction between the 3BP2 SH2 domain and CD19. Figure 7C shows that phosphotyrosines 403 and 443 are capable of mediating this interaction.

To confirm this result, we utilized Daudi cells transfected with one of three chimeric CD4:CD19 receptors (26) which contain either the wild-type cytoplasmic domain of CD19, the cytoplasmic domain in which all nine tyrosine residues are mutated to phenylalanine (ALL F), or the cytoplasmic domain in which tyrosines 403 and 443 have been mutated to phenylalanine (Y403/443F) (23). We observed that the 3BP2 SH2 domain bound to the wild-type CD4:CD19 chimera but not to the ALL F mutant or the Y403/443F mutant receptor (Fig. 7D). These observations demonstrate that CD19 and 3BP2 form an inducible protein complex mediated by tyrosine 403, tyrosine 443, or both.

DISCUSSION

In this report, we showed that 3BP2 is required for optimal signaling through the B-cell antigen receptor and is part of the CD19 costimulatory complex. 3BP2 has a distinctive function in B lymphocytes involved in the TI-2 humoral response. Mice lacking 3BP2 have diminished peritoneal B1 B cells and accumulate MZ B cells which demonstrate enhanced sensitivity to antigen receptor-induced cell death in vitro.

B1 B cells and MZ B cells control the humoral response to TI-2 multivalent antigens (22, 25). TI-2 immune responses occur in the absence of T-cell help but are dependent on optimal activation of the BCR together with BAFF signals elaborated by macrophages and dendritic cells (5, 9, 24, 48). We have shown that $3BP2^{-/-}$ splenic B cells and MZ B cells fail to proliferate, survive, and signal optimally following antigen receptor activation. Consistent with these data, overexpression of 3BP2 augmented BCR-mediated NFAT activation as measured by a luciferase reporter assay, while treatment of Raji cells with 3BP2 small interfering RNA attenuated BCR signaling (12). Our data would support a model in which the B1 and MZ B-cell populations are diminished in numbers or function or both in the absence of 3BP2, leading to a defective TI-2 response in vivo.

The modest increase in MZ B cells observed in the $3BP2^{-/-}$ mice may also be a reflection of suboptimal BCR signaling. One model of MZ B-cell development argues that nascent transitional B cells must receive a BAFF survival signal (32, 38, 39) and a BCR signal sufficient in strength to initiate a FO B-cell developmental program. Those B cells that survive because of BAFF but receive a weak BCR signal then become receptive to inductive signals through Notch2 that support the development of MZ B cells (37). The accumulation of MZ B cells observed in the $3BP2^{-/-}$ mice may result from a failure to maximally activate proximal signal transduction pathways downstream of the BCR, thereby promoting a developmental program favoring MZ B-cell commitment. In distinction to MZ B-cell development, constitutive and optimal BCR signals are required for establishing normal numbers of B1 B cells in the adult animal (1, 18, 20). In this context, the weak BCR signal of $3BP2^{-/-}$ B cells likely contributes to the decreased number of peritoneal B1 B cells found in $3BP2^{-/-}$ mice. Therefore, in the absence of 3BP2, the suboptimal BCR signal affects the developmental pathway of peripheral B cells, MZ B and B1 B cells, and impairs the in vitro survival and in vivo function of MZ B cells in response to BCR cross-linking.

In order to define the biochemical defect underlying the B-cell defects observed in the $3BP2^{-/-}$ mice, we examined the activity and phosphorylation status of a number of canonical signaling molecules downstream of the BCR in $3BP2^{-/-}$ B cells. 3BP2 was identified as a Syk tyrosine kinase binding protein (6) and as a Syk substrate (12). We observed that both the induction and duration of Syk phosphorylation were attenuated in $3BP2^{-/-}$ B cells compared to control cells. However, we observed that there was no effect on the induction of Abl, Erk, JNK, Akt, or PLC-γ2 in $3BP2^{-/-}$ B cells following BCR cross-linking. Although PLC-γ2 phosphorylation was normal, $3BP2^{-/-}$ B cells had reduced calcium flux in response to BCR cross-linking. What could account for the defect in calcium flux in the face of normal PLC-γ2 phosphorylation in $3BP2^{-/-}$ B cells? One possibility is that the production of the PLC-γ2 substrate, phosphatidylinositol-4,5-bisphosphate (PIP_2), is not normal in $3BP2^{-/-}$ B cells. Previous studies demonstrated that CD19 cross-linking induces the de novo synthesis of PIP_2 required to replenish the rapid depletion of PIP_2 by PLC-γ2 (31, 36, 47). We are currently investigating whether the production of PIP_2 is normal in $3BP2^{-/-}$ B cells.

In an attempt to determine how 3BP2 might couple to the BCR signaling machinery, we have shown that endogenous 3BP2 binds inducibly to CD19 following BCR cross-linking at sites previously reported to bind to the Fyn tyrosine kinase (3). The CD19 coreceptor complex, which includes CD21 and CD81, reduces the threshold of BCR activation by up to 10^4-fold (11). CD19 provides this critical signal through its engagement and activation of phosphatidylinositol 3-kinase (44), Vav (31), Lyn (46), and Fyn (3). CD19 is also required for maximum induction of calcium flux (2, 8). 3BP2 may thus be a necessary component of the CD19 signaling complex such that in the absence of 3BP2 the CD19 costimulatory signal is weakened, leading to a diminished BCR signal.

Recently another report describing the B-cell phenotype in 3BP2-deficient mice has been published (7). Consistent with our findings, de la Fuente et al. similarly showed that $3BP2^{-/-}$ B cells demonstrated a proliferation defect and impaired calcium mobilization in response to BCR cross-linking. In distinction to our findings, however, they did not observe a defect in the TI-2 humoral response or a perturbation in the B1 or MZ B-cell populations. Moreover, they did not observe altered survival of B cells in the absence of 3BP2. The principal biochemical abnormalities observed in their study included defects in NFATp dephosphorylation and JNK phosphorylation. The differences in our two phenotypes may result from differences in our respective targeting strategies, the generation number backcrossed onto the C57BL/6 strain, and local variations in microbial environments of the animal colonies.

We have demonstrated that the 3BP2 adapter protein is a component of the CD19 costimulatory complex and is essential for optimum BCR signaling required for normal peritoneal B1 and MZ B-cell development and TI-2 antigen response.

ACKNOWLEDGMENTS

We thank Marcel Deckert, Michael Ratcliffe, Andre Veillette, Robert Carter, Michael Cooke, and Andrew Su (Novartis) for helpful discussions and comments.

This research was supported by the CIHR, an NCIC Terry Fox Program Project grant, NSERC, and OGSST. R.R. was supported as a CIHR Scientist.

REFERENCES

1. **Cariappa, A., and S. Pillai.** 2002. Antigen-dependent B-cell development. Curr. Opin. Immunol. **14:**241–249.
2. **Carter, R. H., D. A. Tuveson, D. J. Park, S. G. Rhee, and D. T. Fearon.** 1991. The CD19 complex of B lymphocytes. Activation of phospholipase C by a protein tyrosine kinase-dependent pathway that can be enhanced by the membrane IgM complex. J. Immunol. **147:**3663–3671.
3. **Chalupny, N. J., A. Aruffo, J. M. Esselstyn, P. Y. Chan, J. Bajorath, J. Blake, L. K. Gilliland, J. A. Ledbetter, and M. A. Tepper.** 1995. Specific binding of Fyn and phosphatidylinositol 3-kinase to the B cell surface glycoprotein CD19 through their src homology 2 domains. Eur. J. Immunol. **25:**2978–2984.
4. **Cicchetti, P., B. J. Mayer, G. Thiel, and D. Baltimore.** 1992. Identification of a protein that binds to the SH3 region of Abl and is similar to Bcr and GAP-rho. Science **257:**803–806.
5. **Craxton, A., D. Magaletti, E. J. Ryan, and E. A. Clark.** 2003. Macrophage- and dendritic cell-dependent regulation of human B-cell proliferation requires the TNF family ligand BAFF. Blood **101:**4464–4471.
6. **Deckert, M., S. Tartare-Deckert, J. Hernandez, R. Rottapel, and A. Altman.** 1998. Adaptor function for the Syk kinase-interacting protein 3BP2 in IL-2 gene activation. Immunity **9:**595–605.
7. **de la Fuente, M. A., L. Kumar, B. Lu, and R. S. Geha.** 2006. 3BP2 deficiency impairs the response of B cells, but not T cells, to antigen receptor ligation. Mol. Cell. Biol. **26:**5214–5225.
8. **Dempsey, P. W., M. E. Allison, S. Akkaraju, C. C. Goodnow, and D. T. Fearon.** 1996. C3d of complement as a molecular adjuvant: bridging innate and acquired immunity. Science **271:**348–350.
9. **Fagarasan, S., and T. Honjo.** 2000. T-independent immune response: new aspects of B cell biology. Science **290:**89–92.
10. **Fang, W., D. L. Mueller, C. A. Pennell, J. J. Rivard, Y. S. Li, R. R. Hardy, M. S. Schlissel, and T. W. Behrens.** 1996. Frequent aberrant immunoglobulin gene rearrangements in pro-B cells revealed by a bcl-xL transgene. Immunity **4:**291–299.
11. **Fearon, D. T., and M. C. Carroll.** 2000. Regulation of B lymphocyte responses to foreign and self-antigens by the CD19/CD21 complex. Annu. Rev. Immunol. **18:**393–422.
12. **Foucault, I., S. Le Bras, C. Charvet, C. Moon, A. Altman, and M. Deckert.** 2005. The adaptor protein 3BP2 associates with VAV guanine nucleotide exchange factors to regulate NFAT activation by the B-cell antigen receptor. Blood **105:**1106–1113.
13. **Fujimoto, M., J. C. Poe, P. J. Jansen, S. Sato, and T. F. Tedder.** 1999. CD19 amplifies B lymphocyte signal transduction by regulating Src-family protein tyrosine kinase activation. J. Immunol. **162:**7088–7094.
14. **Grossmann, M., L. A. O'Reilly, R. Gugasyan, A. Strasser, J. M. Adams, and S. Gerondakis.** 2000. The anti-apoptotic activities of Rel and RelA required during B-cell maturation involve the regulation of Bcl-2 expression. EMBO J. **19:**6351–6360.
15. **Grumont, R. J., I. J. Rourke, and S. Gerondakis.** 1999. Rel-dependent induction of A1 transcription is required to protect B cells from antigen receptor ligation-induced apoptosis. Genes Dev. **13:**400–411.
16. **Grynkiewicz, G., M. Poenie, and R. Y. Tsien.** 1985. A new generation of Ca2+ indicators with greatly improved fluorescence properties. J. Biol. Chem. **260:**3440–3450.
17. **Jevremovic, D., D. D. Billadeau, R. A. Schoon, C. J. Dick, and P. J. Leibson.** 2001. Regulation of NK cell-mediated cytotoxicity by the adaptor protein 3BP2. J. Immunol. **166:**7219–7228.
18. **Jumaa, H., B. Wollscheid, M. Mitterer, J. Wienands, M. Reth, and P. J. Nielsen.** 1999. Abnormal development and function of B lymphocytes in mice deficient for the signaling adaptor protein SLP-65. Immunity **11:**547–554.
19. **Kendrick, T. S., R. J. Lipscombe, O. Rausch, S. E. Nicholson, J. E. Layton, L. C. Goldie-Cregan, and M. A. Bogoyevitch.** 2004. Contribution of the membrane-distal tyrosine in intracellular signaling by the granulocyte colony-stimulating factor receptor. J. Biol. Chem. **279:**326–340.
20. **Khan, W. N., F. W. Alt, R. M. Gerstein, B. A. Malynn, I. Larsson, G. Rathbun, L. Davidson, S. Muller, A. B. Kantor, L. A. Herzenberg, et al.** 1995. Defective B cell development and function in Btk-deficient mice. Immunity **3:**283–299.
21. **Kraal, G., K. Schornagel, P. R. Streeter, B. Holzmann, and E. C. Butcher.** 1995. Expression of the mucosal vascular addressin, MAdCAM-1, on sinus-lining cells in the spleen. Am. J. Pathol. **147:**763–771.
22. **Lane, P. J., D. Gray, S. Oldfield, and I. C. MacLennan.** 1986. Differences in the recruitment of virgin B cells into antibody responses to thymus-dependent and thymus-independent type-2 antigens. Eur. J. Immunol. **16:**1569–1575.
23. **Li, X., D. Sandoval, L. Freeberg, and R. H. Carter.** 1997. Role of CD19 tyrosine 391 in synergistic activation of B lymphocytes by coligation of CD19 and membrane Ig. J. Immunol. **158:**5649–5657.
24. **Litinskiy, M. B., B. Nardelli, D. M. Hilbert, B. He, A. Schaffer, P. Casali, and A. Cerutti.** 2002. DCs induce CD40-independent immunoglobulin class switching through BLyS and APRIL. Nat. Immunol. **3:**822–829.
25. **Martin, F., and J. F. Kearney.** 2000. B-cell subsets and the mature preimmune repertoire. Marginal zone and B1 B cells as part of a "natural immune memory." Immunol. Rev. **175:**70–79.
26. **Matsumoto, A. K., D. R. Martin, R. H. Carter, L. B. Klickstein, J. M. Ahearn, and D. T. Fearon.** 1993. Functional dissection of the CD21/CD19/TAPA-1/Leu-13 complex of B lymphocytes. J. Exp. Med. **178:**1407–1417.
27. **Mond, J. J., A. Lees, and C. M. Snapper.** 1995. T cell-independent antigens type 2. Annu. Rev. Immunol. **13:**655–692.
28. **Nagar, B., O. Hantschel, M. A. Young, K. Scheffzek, D. Veach, W. Bornmann, B. Clarkson, G. Superti-Furga, and J. Kuriyan.** 2003. Structural basis for the autoinhibition of c-Abl tyrosine kinase. Cell **112:**859–871.
29. **Oliver, A. M., F. Martin, G. L. Gartland, R. H. Carter, and J. F. Kearney.** 1997. Marginal zone B cells exhibit unique activation, proliferative and immunoglobulin secretory responses. Eur. J. Immunol. **27:**2366–2374.
30. **Opferman, J. T., A. Letai, C. Beard, M. D. Sorcinelli, C. C. Ong, and S. J. Korsmeyer.** 2003. Development and maintenance of B and T lymphocytes requires antiapoptotic MCL-1. Nature **426:**671–676.
31. **O'Rourke, L. M., R. Tooze, M. Turner, D. M. Sandoval, R. H. Carter, V. L. Tybulewicz, and D. T. Fearon.** 1998. CD19 as a membrane-anchored adaptor protein of B lymphocytes: costimulation of lipid and protein kinases by recruitment of Vav. Immunity **8:**635–645.
32. **Pillai, S., A. Cariappa, and S. T. Moran.** 2005. Marginal zone B cells. Annu. Rev. Immunol. **23:**161–196.
33. **Ren, R., B. J. Mayer, P. Cicchetti, and D. Baltimore.** 1993. Identification of a ten-amino acid proline-rich SH3 binding site. Science **259:**1157–1161.
34. **Saborit-Villarroya, I., J. M. Del Valle, X. Romero, E. Esplugues, P. Lauzurica, P. Engel, and M. Martin.** 2005. The adaptor protein 3BP2 binds human CD244 and links this receptor to Vav signaling, ERK activation, and NK cell killing. J. Immunol. **175:**4226–4235.
35. **Sada, K., S. M. Miah, K. Maeno, S. Kyo, X. Qu, and H. Yamamura.** 2002. Regulation of FcepsilonRI-mediated degranulation by an adaptor protein 3BP2 in rat basophilic leukemia RBL-2H3 cells. Blood **100:**2138–2144.
36. **Saito, K., K. F. Tolias, A. Saci, H. B. Koon, L. A. Humphries, A. Scharenberg, D. J. Rawlings, J. P. Kinet, and C. L. Carpenter.** 2003. BTK regulates PtdIns-4,5-P2 synthesis: importance for calcium signaling and PI3K activity. Immunity **19:**669–678.
37. **Saito, T., S. Chiba, M. Ichikawa, A. Kunisato, T. Asai, K. Shimizu, T. Yamaguchi, G. Yamamoto, S. Seo, K. Kumano, E. Nakagami-Yamaguchi, Y. Hamada, S. Aizawa, and H. Hirai.** 2003. Notch2 is preferentially expressed in mature B cells and indispensable for marginal zone B lineage development. Immunity **18:**675–685.
38. **Schiemann, B., J. L. Gommerman, K. Vora, T. G. Cachero, S. Shulga-Morskaya, M. Dobles, E. Frew, and M. L. Scott.** 2001. An essential role for BAFF in the normal development of B cells through a BCMA-independent pathway. Science **293:**2111–2114.
39. **Schneider, P., H. Takatsuka, A. Wilson, F. Mackay, A. Tardivel, S. Lens, T. G. Cachero, D. Finke, F. Beermann, and J. Tschopp.** 2001. Maturation of marginal zone and follicular B cells requires B cell activating factor of the tumor necrosis factor family and is independent of B cell maturation antigen. J. Exp. Med. **194:**1691–1697.
40. **Songyang, Z., S. E. Shoelson, J. McGlade, P. Olivier, T. Pawson, X. R. Bustelo, M. Barbacid, H. Sabe, H. Hanafusa, T. Yi, et al.** 1994. Specific motifs recognized by the SH2 domains of Csk, 3BP2, fps/fes, GRB-2, HCP, SHC, Syk, and Vav. Mol. Cell. Biol. **14:**2777–2785.
41. **Southgate, J., U. Sarma, J. V. Townend, J. Barron, and A. M. Flanagan.** 1998. Study of the cell biology and biochemistry of cherubism. J. Clin. Pathol. **51:**831–837.
42. **Su, A. I., T. Wiltshire, S. Batalov, H. Lapp, K. A. Ching, D. Block, J. Zhang, R. Soden, M. Hayakawa, G. Kreiman, M. P. Cooke, J. R. Walker, and J. B. Hogenesch.** 2004. A gene atlas of the mouse and human protein-encoding transcriptomes. Proc. Natl. Acad. Sci. USA. **101:**6062–6067.
43. **Tedder, T. F., and C. M. Isaacs.** 1989. Isolation of cDNAs encoding the CD19 antigen of human and mouse B lymphocytes. A new member of the immunoglobulin superfamily. J. Immunol. **143:**712–717.
44. **Tuveson, D. A., R. H. Carter, S. P. Soltoff, and D. T. Fearon.** 1993. CD19 of B cells as a surrogate kinase insert region to bind phosphatidylinositol 3-kinase. Science **260:**986–989.
45. **Ueki, Y., V. Tiziani, C. Santanna, N. Fukai, C. Maulik, J. Garfinkle, C. Ninomiya, C. doAmaral, H. Peters, M. Habal, L. Rhee-Morris, J. B. Doss, S. Kreiborg, B. R. Olsen, and E. Reichenberger.** 2001. Mutations in the gene encoding c-Abl-binding protein SH3BP2 cause cherubism. Nat. Genet. **28:**125–126.
46. **van Noesel, C. J., A. C. Lankester, G. M. van Schijndel, and R. A. van Lier.** 1993. The CR2/CD19 complex on human B cells contains the src-family kinase Lyn. Int. Immunol. **5:**699–705.

47. **Vigorito, E., E. Clayton, and M. Turner.** 2004. BCR activation of PI3K is Vav-independent in murine B cells. Biochem. Soc. Trans. **32:**781–784.
48. **von Bulow, G. U., J. M. van Deursen, and R. J. Bram.** 2001. Regulation of the T-independent humoral response by TACI. Immunity **14:**573–582.
49. **Wang, Y., S. R. Brooks, X. Li, A. N. Anzelon, R. C. Rickert, and R. H. Carter.** 2002. The physiologic role of CD19 cytoplasmic tyrosines. Immunity **17:**501–514.
50. **Woodring, P. J., T. Hunter, and J. Y. Wang.** 2005. Mitotic phosphorylation rescues Abl from F-actin-mediated inhibition. J. Biol. Chem. **280:**10318–10325.
51. **Zipfel, P. A., M. Grove, K. Blackburn, M. Fujimoto, T. F. Tedder, and A. M. Pendergast.** 2000. The c-Abl tyrosine kinase is regulated downstream of the B cell antigen receptor and interacts with CD19. J. Immunol. **165:**6872–6879.